Dynamical exchange-correlation potentials in the spin channel for the two-dimensional electron liquid

Zhixin Qian
Department of Physics and State Key Laboratory for Mesoscopic Physics, Peking University, Beijing 100871, China
(Received 11 January 2005; revised manuscript received 5 May 2005; published 10 August 2005)

The exchange-correlation kernel in the spin channel in an electron liquid has the structure $f_{xc,-}^{L,T}(q,\omega) \overset{q\to 0}{\to} A(\omega)/q^2 + B^{L,T}(\omega)$ in the limit of the long wavelength. Here L denotes the longitudinal component and T the transverse component relative to the direction of the wave vector $\mathbf{q}$. A collection of exact results for $A(\omega)$ and $B^{L,T}(\omega)$ is obtained at limiting low and high frequency, respectively, in two dimensions. Based on these results, we further give approximate interpolations for $A(\omega)$ and $B^{L,T}(\omega)$ at all frequencies in the paramagnetic case.

DOI: 10.1103/PhysRevB.72.075115 PACS number(s): 71.10.Ay, 72.10.−d

I. INTRODUCTION

Two-dimensional (2D) electron systems, particularly those realized at the interfaces of semiconductor heterostructures,[1] present a field for the study of many-body effects in the electron liquid with variable density. Extensive progress has been made in this field.[1,2] But the difficult subject of the exchange-correlation (xc) effects in many-electron systems continues to be a challenge, particularly due to the enhanced correlation effects in comparison to the traditional three-dimensional (3D) electron liquid.

In most theoretical studies,[3–5] the xc effects in the homogeneous electron liquid are taken into account by the use of the local-field factor $G^{L,T}(q,\omega)$ or the more specific spin-resolved one of $G_{\sigma\sigma'}^{L,T}(q,\omega)$, where L and T denote the longitudinal and transverse components relative to the direction of $\mathbf{q}$, respectively; $\sigma=1$ for $\uparrow$ spin and $\sigma=-1$ for $\downarrow$ spin. This approach is conventionally taken in the studies of the 2D case as well. The local-field factor also plays a central role in time-dependent (spin) density functional theory [TD(S)DFT][6–9] and the recently proposed scheme of time-dependent (spin) current-density functional theory [TD(S)CDFT],[10–13] in which the homogeneous electron-liquid model is normally taken as a reference system. In TD(S)DFT [or TD(S)CDFT], one frequently uses, instead, the equivalent xc kernel, defined as

$$f_{xc,\sigma\sigma'}^{L,T}(q,\omega) = -v(q)G_{\sigma\sigma'}^{L,T}(q,\omega). \tag{1}$$

Here $v(q)$ is the Fourier transform of the Coulomb interaction, and $v(q)=2\pi e^2/q$ in 2D. The scheme of TD(S)CDFT was proposed to overcome several intrinsic difficulties in the conventional TD(S)DFT and has recently found interesting applications in the studies of optical spectra of solids,[14] the polarizability of long polymer chains,[15] and the excitation energies for molecules[16] and oligomers.[17]

It has been shown that,[18,19] in both 3D and 2D, the xc kernel in the spin channel, defined as

$$f_{xc,-}^{L,T}(q,\omega) = \sum_{\sigma\sigma'} \frac{n_\sigma n_{\sigma'}}{n^2} \sigma\sigma' f_{xc,\sigma\sigma'}^{L,T}(q,\omega), \tag{2}$$

where n_σ is the spin-resolved density and $n=n_\uparrow+n_\downarrow$ is the charge density, has a singular structure, as follows:

$$f_{xc,-}^{L,T}(q,\omega) = \frac{A(\omega)}{q^2} + B^{L,T}(\omega) + \cdots, \tag{3}$$

in the limit of small q. It has been further shown that $A(\omega)$ is well behaved in 3D,[18] but that the real part of it is logarithmically divergent at high frequency in 2D.[19] Correspondingly, its imaginary part goes as a constant at high frequency in 2D. Several other interesting results for $A(\omega)$ and $B^{L,T}(\omega)$ at limiting high frequency in 2D have also been exactly found for arbitrary spin polarization in Ref. 19. Some other properties are found in Refs. 20 and 21.

In the studies of the local-field factor or the equivalent xc kernel, one usually resorts to fully perturbative calculations (for example, in Refs. 22 and 23), or some self-consistent calculations (for example, in Refs. 24 and 25). Such calculations are, however, usually rather complicated and must be carried through with some approximations that are not always controllable. There is an approach[18,26–29] at variance with the fully perturbative calculations, in which some exact or definitely reliable limiting results and sum rules for the local-field factor are established, and further interpolated into approximate expressions. Such an approach turns out to be rather efficient. In this paper, we attempt to take this approach to obtain approximations to $f_{xc,-}^{L,T}(q,\omega)$ for arbitrary frequency at long wavelength in a paramagnetic 2D electron liquid.

The high-frequency structures of $A(\omega)$ were obtained analytically in Ref. 19, while the low-frequency structure of $\mathrm{Re}\,A(\omega)$ was obtained in Ref. 30. In this paper, we will calculate analytically the low-frequency limit of $\mathrm{Im}\,A(\omega)$, which is found to be $\sim\omega^3 \ln \omega/E_F$, where E_F is the Fermi energy.

The infinite frequency limit of $\mathrm{Re}\,B^{L,T}(\omega)$ has been obtained in Ref. 19. Part of this paper is devoted to studying several other properties of $B^{L,T}(\omega)$. To this end, we evaluate $\mathrm{Im}\,B^{L,T}(\omega)$ analytically and find it to decrease as $1/\omega$ at large ω. This asymptotic behavior is exact at high frequency. The zero-frequency limits of $\mathrm{Re}\,B^{L,T}(\omega)$ and low-frequency limits of $\mathrm{Im}\,B^{L,T}(\omega)$ are also obtained in this paper.

These limiting properties enable us to further obtain approximate interpolations for the imaginary parts $\mathrm{Im}\,A(\omega)$ and

 ©2005 The American Physical Society

Im $B^{L,T}(\omega)$ at all frequencies. The corresponding real parts are then calculated from them via the Kramers-Krönig dispersion relations. By the use of these interpolations and those for the charge channel in Ref. 29, we further calculate the limiting small momentum structures of plasmon dispersion, static structure factor, and static local-field factor, and compare them with the results reported in the literature.

The analytical results obtained in this paper reflect definitive progress in the study of the 2D many-electron systems. These results and the approximate interpolations for $A(\omega)$ and $B^{L,T}(\omega)$ are also useful in the practical implements of time-dependent spin-density functional theory in two-dimensional or quasi-two-dimensional systems.

We organize the paper as follows: The exact properties for $A(\omega)$ and $B^{L,T}(\omega)$ are summarized in Sec. II. The derivations for the newly established properties are given in Sec. III. In Sec. IV, we present our interpolations for both $A(\omega)$ and $B^{L,T}(\omega)$. We summarize the paper in Sec. V. In the Appendix, we calculate the plasmon dispersion, the static structure factor, and the static local-field factor in the small momentum regime, and compare them with previous calculations.

II. EXACT PROPERTIES

In this section, we list the exact properties of $A(\omega)$ and $B^{L,T}(\omega)$ in 2D. The details of derivations leading to them will be presented in the next section.

A. Exact properties for $A(\omega)$

The high-frequency behavior of Im $A(\omega)$ is (Ref. 19)

$$\mathrm{Im}\, A(\omega) \overset{\omega\to\infty}{\to} -\frac{1}{2}\pi^2 m e^4. \tag{4}$$

In other words, Im $A(\omega)$ goes as a constant at large frequency. Correspondingly, the real part Re $A(\omega)$ diverges logarithmically at large frequency as (Ref. 19)

$$\mathrm{Re}\, A(\omega) \overset{\omega\to\infty}{\to} \pi m e^4 \ln \omega/E_F. \tag{5}$$

We note that the preceding result is accurate only to the leading logarithmic order.

In addition, Re $A(\omega)$ vanishes at zero frequency as ω^2,[30]

$$\lim_{\omega\to 0} \mathrm{Re}\, A(\omega) = 0, \tag{6}$$

$$1 - \lim_{\omega\to 0} \frac{n\, \mathrm{Re}\, A(\omega)}{m\omega^2} = \frac{1+F_1^s/2}{1+F_1^a/2}, \tag{7}$$

where F_l^s and F_l^a are the spin-symmetric and spin-antisymmetric Landau parameters, respectively. At the high-density limit,

$$\mathrm{Im}\, A(\omega) \overset{\omega\to 0}{\to} \frac{1}{3}\left[\frac{m^2 e^2}{\pi n(2k_F + k_s)}\right]^2 \omega^3 \ln\frac{\omega}{E_F}, \tag{8}$$

where k_s is the screening wave vector, $k_s = 2/a_0$, k_F is the Fermi wave vector, and a_0 is the Bohr radius.

B. Exact properties for $B^{L,T}(\omega)$

The high-frequency behavior of Im $B^{L,T}(\omega)$ is

$$\mathrm{Im}\, B^{L,T}(\omega) \overset{\omega\to\infty}{\to} -c^{L,T}\frac{\pi^2 e^4}{\omega}, \tag{9}$$

where $c^L = 9/32$, $c^T = 3/32$.

The infinite frequency limit of Re $B^{L,T}(\omega)$ is (Ref. 19)

$$\mathrm{Re}\, B^{L,T}(\infty) = \alpha^{L,T}\frac{t_c}{n} - \frac{\beta^{L,T}}{2}\int d\mathbf{r} v(\mathbf{r}) g_-(r), \tag{10}$$

where $\alpha^L = 3$, $\alpha^T = 1$; $\beta^L = -\frac{5}{8}$, $\beta^T = \frac{1}{8}$; t_c is the correlation kinetic energy per particle, and $g_-(r) = \sum_{\sigma\sigma'}(n_\sigma n_{\sigma'}/n^2)\sigma\sigma' g_{\sigma\sigma'}(r)$, with $g_{\sigma\sigma'}(r)$ the spin-resolved pair-correlation density.

The zero-frequency limits of Re $B^{L,T}(\omega)$ are related to the Landau parameters as follows:

$$\mathrm{Re}\, B^L(0) = \frac{E_F}{4n}\frac{F_2^a + 4F_0^a - 3F_1^s}{1 + (F_1^s/2)}, \tag{11}$$

and

$$\mathrm{Re}\, B^T(0) = \frac{E_F}{4n}\frac{F_2^a - F_1^s}{1 + (F_1^s/2)}. \tag{12}$$

It was proved in Ref. 18 that Im $B^{L,T}(\omega) = \mathrm{Im}\, f_{xc}^{L,T}(q=0,\omega)$ in 3D. The proof also simply holds in 2D. Thus, from the result of Eq. (15) in Ref. 29, we have the following low-frequency behavior of Im $B^{L,T}(\omega)$:

$$\lim_{\omega\to 0}\frac{\mathrm{Im}\, B^{L,T}(\omega)}{\omega} = -\left(\frac{me^2}{n\pi}\right)^2 S^{L,T}, \tag{13}$$

where

$$S^L = \frac{1}{6}\left[-\frac{\pi}{4} + \frac{3-\lambda^2}{2-\lambda^2}\ln(\lambda+1) - \frac{\lambda}{1+\lambda} + \frac{1}{2-\lambda^2}f(\lambda)\right], \tag{14}$$

and

$$S^T = S^L. \tag{15}$$

In the preceding expression, $\lambda = 2k_F/k_s$, and

$$f(\lambda) = 2\sqrt{1-\lambda^2}\tan^{-1}\sqrt{\frac{1-\lambda}{1+\lambda}}\theta(1-\lambda) + \sqrt{\lambda^2-1}\ln\left(\frac{\sqrt{\lambda+1}-\sqrt{\lambda-1}}{\sqrt{\lambda+1}+\sqrt{\lambda-1}}\right)\theta(\lambda-1). \tag{16}$$

Equation (13) is perturbative, and therefore strictly valid only in the high-density limit. However, the following relation:

$$\lim_{\omega\to 0}\frac{\mathrm{Im}\, B^T(\omega)}{\omega} = \lim_{\omega\to 0}\frac{\mathrm{Im}\, B^L(\omega)}{\omega} \tag{17}$$

is nonperturbative and, as such, is expected to hold at all densities. We note that a relation similar to Eq. (17) holds in 3D [see Eq. (23) in Ref. 18].

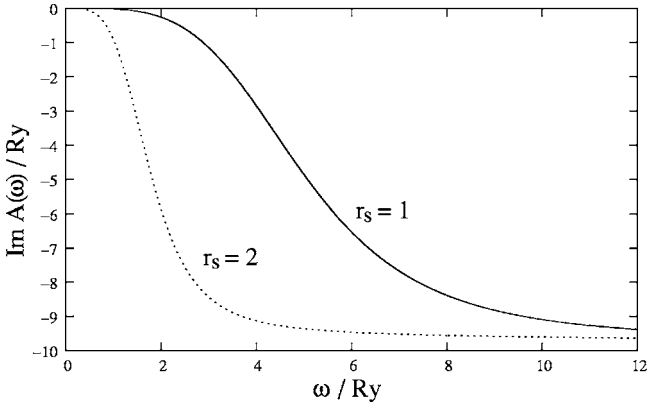

FIG. 1. Imaginary part of $A(\omega)$ at $r_s=1,2$ as functions of ω.

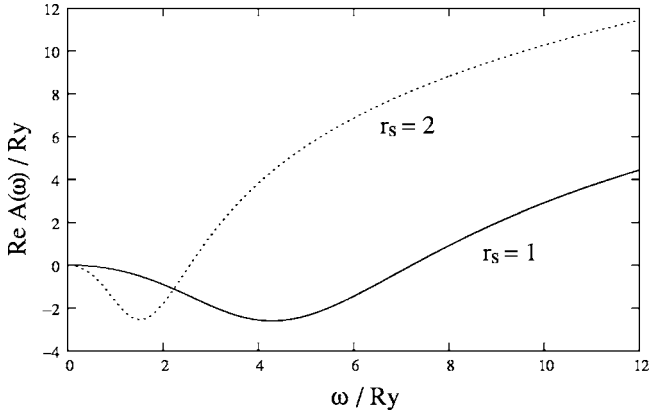

FIG. 2. Real part of $A(\omega)$ at $r_s=1,2$ as functions of ω.

III. DERIVATIONS

A. Low-frequency limit of Im $A(\omega)$

The high-frequency results for $\mathrm{Im}\,A(\omega)$ and $\mathrm{Re}\,A(\omega)$, shown in Eqs. (4) and (5), respectively, have been derived in Ref. 19. The results of Eqs. (6) and (7) are established in Ref. 30. Here, we only briefly give the derivation for Eq. (8)—the low-frequency limit of $\mathrm{Im}\,A(\omega)$. Equation (8) is established within the mode-decoupling approximation, which is exact only in the high-density limit.[13,22,31] The analytic form of this approximation to $\mathrm{Im}\,A(\omega)$ is given by Eq. (14) of Ref. 13, which, in the paramagnetic case, reduces in 2D to

$$\mathrm{Im}\,A(\omega) = -\frac{2}{n^2\Omega}\sum_{\mathbf{q}} v_{\mathbf{q}}^2 q^2 \int_0^{\omega}\frac{d\omega'}{\pi} \times \frac{\mathrm{Im}\,\chi_{0\uparrow}(q,\omega-\omega')\mathrm{Im}\,\chi_{0\uparrow}(q,\omega')}{|\epsilon(q,\omega-\omega')|^2|\epsilon(q,\omega')|^2}\{[1+\Theta(q,\omega-\omega')] \times[1+\Theta(q,\omega')]-\Theta(q,\omega-\omega')\Theta(q,\omega')\}, \quad (18)$$

where $\epsilon(q,\omega)$ is the dielectric function; $\Theta(q,\omega)=2v(q)\times[-\mathrm{Re}\,\chi_{0\uparrow}(q,\omega)+v(q)|\chi_{0\uparrow}(q,\omega)|^2]$; and $\chi_{0\uparrow}(q,\omega)$ is the Lindhard function for just one spin component. In the paramagnetic case,

$$\mathrm{Im}\,\chi_{0\uparrow}(q,\omega) = \frac{m}{2\pi q^2}\{\theta[k_F^2q^2-(m\omega+q^2/2)^2]\sqrt{k_F^2q^2-(m\omega+q^2/2)^2}-\theta[k_F^2q^2-(m\omega-q^2/2)^2]\sqrt{k_F^2q^2-(m\omega-q^2/2)^2}\}. \quad (19)$$

To leading order in ω, for small ω, in Eq. (18) simplies to

$$\mathrm{Im}\,A(\omega) = -\frac{2}{n^2\Omega}\sum_{\mathbf{q}} v_{\mathbf{q}}^2 q^2 \frac{1}{|\epsilon(q,0)|^2}\int_0^{\omega}\frac{d\omega'}{\pi}\,\mathrm{Im}\,\chi_{0\uparrow}(q,\omega-\omega')\mathrm{Im}\chi_{0\uparrow}(q,\omega'). \quad (20)$$

On the other hand, for small ω,

$$\mathrm{Im}\,\chi_{0\uparrow}(q,\omega) = -\frac{m^2\omega}{\pi q\sqrt{4k_F^2-q^2}}. \quad (21)$$

Substituting the preceding expression into Eq. (20), one obtains, after some algebra,

$$\mathrm{Im}\,A(\omega)\overset{\omega\to 0}{\to} -\frac{1}{\Omega}\left(\frac{2m^2}{\pi n}\right)^2\int_{\omega/2}^{\omega}\frac{d\omega'}{\pi}\omega'(\omega-\omega') \times\sum_{\mathbf{q}} v^2(q)\frac{1}{|\epsilon(q,0)|^2}\frac{1}{4k_F^2-q^2}\theta(k_Fq-q^2/2-\omega'). \quad (22)$$

Making use of the random-phase approximation (RPA) to the static dielectric function, one obtains, after some straightforward calculations, the result of Eq. (8).

B. High-frequency limit of Im $B^{L,T}(\omega)$

The high-frequency limit of $\mathrm{Im}\,B^{L,T}(\omega)$ in 3D was established in Ref. 18. In this subsection, we extend it to the 2D case. In fact, to leading order at high frequency, the imaginary part of the xc kernel tensor $\mathrm{Im}\,f_{xc,-}^{ij}(\mathbf{q},\omega)$ in the spin channel, where i and j are Cartesian indices, can be written as a combination of two parts,

$$\mathrm{Im}\,f_{xc,-}^{ij}(\mathbf{q},\omega) = \mathrm{Im}\,f_{xc,-}^{ij,a}(\mathbf{q},\omega) + \mathrm{Im}\,f_{xc,-}^{ij,b}(\mathbf{q},\omega), \quad (23)$$

where

$$\mathrm{Im}\,f_{xc,-}^{ij,a}(\mathbf{q},\omega) = -\frac{\pi}{2q^2\Omega}\sum_{\mathbf{k}}\delta(\omega-k^2/m-q^2/4m)v(\mathbf{k}-\mathbf{q}/2)(k_i-q_i/2)\times[v(\mathbf{k}-\mathbf{q}/2)(k_j-q_j/2)+v(\mathbf{k}+\mathbf{q}/2)(k_j+q_j/2)], \quad (24)$$

and

$$\mathrm{Im}\,f_{xc,-}^{ij,b}(\mathbf{q},\omega) = \frac{\pi}{4\Omega mq^2}\frac{1}{\omega}\sum_{\mathbf{k}}\delta(\omega-k^2/m)v(\mathbf{k}-\mathbf{q}/2)\mathbf{k}\cdot\mathbf{q}\times\{[-v(\mathbf{k}+\mathbf{q}/2)+v(\mathbf{k}-\mathbf{q}/2)](k_iq_j+k_jq_i)-4v(\mathbf{k}-\mathbf{q}/2)k_ik_j\}. \quad (25)$$

Here, Ω is the area of the system. Equations (24) and (25)

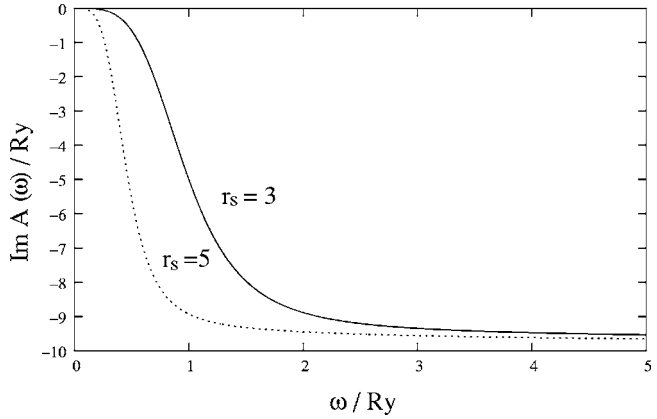

FIG. 3. Imaginary part of $A(\omega)$ at $r_s=3,5$ as functions of ω.

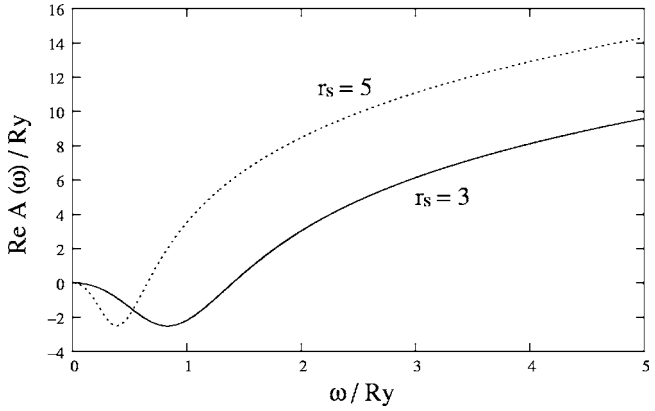

FIG. 4. Real part of $A(\omega)$ at $r_s=3,5$ as functions of ω.

are formally the same as Eqs. (46) and (56) in 3D, and so are the derivations leading to them.[18] In passing, we note a typo of missing $\frac{1}{4}\Sigma_{\sigma\sigma'}\sigma\sigma'$ in Eq. (56) of Ref. 18. We first consider term a. From Eq. (24), we have

$$\mathrm{Im}\, f_{xc,-}^{L,a}(q,\omega) = -\frac{\pi}{4q^4\Omega}\sum_{\mathbf{k}} \delta(\omega - k^2/m - q^2/4m)v^2(k)\frac{1}{k^4} \times [4(\mathbf{k}\cdot\mathbf{q})^2k^4 + 3(\mathbf{k}\cdot\mathbf{q})^4 - 3(\mathbf{k}\cdot\mathbf{q})^2q^2k^2], \tag{26}$$

where we have ignored terms that vanish for $q\to 0$. After carrying out the sum over $\mathbf{k}$ in Eq. (26), one obtains

$$\mathrm{Im}\, f_{xc,-}^{L,a}(q,\omega) = -\frac{m\pi^2e^4}{8q^2}[4 - 3q^2/4m\omega]. \tag{27}$$

Similarly, one can obtain the transverse component as

$$\mathrm{Im}\, f_{xc,-}^{T,a}(q,\omega) = -\frac{m\pi^2e^4}{8q^2}[4 - q^2/4m\omega^2]. \tag{28}$$

Next, we turn to term b. From Eq. (25), we have, to the accuracy of $O(q^0)$,

$$\mathrm{Im}\, f_{xc,-}^{ij,b}(\mathbf{q},\omega) = -\frac{\pi}{\Omega mq^2}\frac{1}{\omega} \sum_{\mathbf{k}} v^2(\mathbf{k})\delta(\omega - k^2/m)\frac{(\mathbf{k}\cdot\mathbf{q})^2}{k^2}k_ik_j. \tag{29}$$

The longitudinal and transverse components can be further evaluated as

$$\mathrm{Im}\, f_{xc,-}^{L,b}(\omega) = -\frac{3\pi^2e^4}{8\omega}, \tag{30}$$

and

$$\mathrm{Im}\, f_{xc,-}^{T,b}(\omega) = -\frac{\pi^2e^4}{8\omega}, \tag{31}$$

respectively. Combining Eqs. (27) and (28) and Eqs. (30) and (31) yields our final results

$$\mathrm{Im}\, f_{xc,-}^{L}(q,\omega) = -\frac{m\pi^2e^4}{32}\left(\frac{16}{q^2} + \frac{9}{m\omega}\right), \tag{32}$$

and

$$\mathrm{Im}\, f_{xc,-}^{T}(q,\omega) = -\frac{m\pi^2e^4}{32}\left(\frac{16}{q^2} + \frac{3}{m\omega}\right). \tag{33}$$

C. Low-frequency limit of Re $B^{L,T}(\omega)$

The low-frequency limit of the xc kernel for the spin channel was related to the Landau parameters in Ref. 18 in 3D. In this subsection, we extend those results to the 2D case.

The response of spin current $\mathbf{j}_a(\mathbf{q},\omega)$ to the perturbation of spin-channel vector potential $\mathbf{A}_a(\mathbf{q},\omega)$ is given by

$$j_a^{L,T}(q,\omega) = \chi_s^{L,T}(q,\omega)A_a^{L,T}(q,\omega), \tag{34}$$

where the spin-channel vector potential $\mathbf{A}_a(\mathbf{q},\omega)$ is defined as

$$\mathbf{A}_a(\mathbf{q},\omega) = \frac{1}{2}[\mathbf{A}_\uparrow(\mathbf{q},\omega) - \mathbf{A}_\downarrow(\mathbf{q},\omega)]. \tag{35}$$

The derivation of the small-q limit of the response function $\chi_s^{L,T}(q,\omega)$ is formally the same as 3D. We therefore only present the final results here,

$$\chi_s^L(q,\omega) - \frac{n}{m_s} \xrightarrow{q\to 0} \frac{3nq^2k_F^2}{4m_s^2m^*\omega^2}\left(1 + \frac{2F_0^a}{3} + \frac{F_2^a}{6}\right), \tag{36}$$

and

$$\chi_s^T(q,\omega) - \frac{n}{m_s} \xrightarrow{q\to 0} \frac{nq^2k_F^2}{4m_s^2m^*\omega^2}\left(1 + \frac{F_2^a}{2}\right). \tag{37}$$

Here, m^* is the effective mass of the quasiparticle and m_s is the spin mass (Ref. 30),

$$\frac{1}{m_s} = \frac{1}{m^*}\left(1 + \frac{1}{2}F_1^a\right). \tag{38}$$

On the other hand, we also have

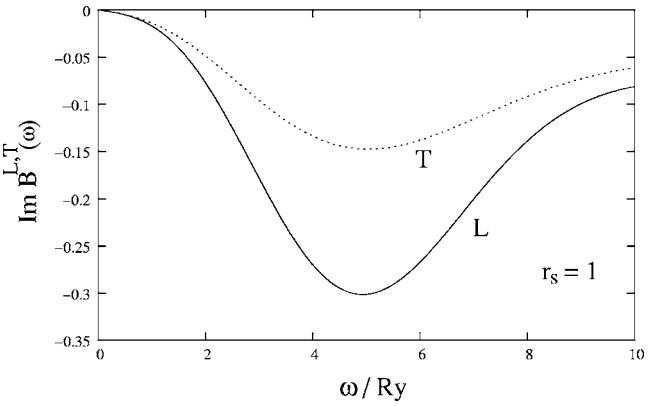

FIG. 5. Imaginary part of $B^L(\omega)$ and $B^T(\omega)$ at $r_s=1$ in units of Ry/n, as functions of ω.

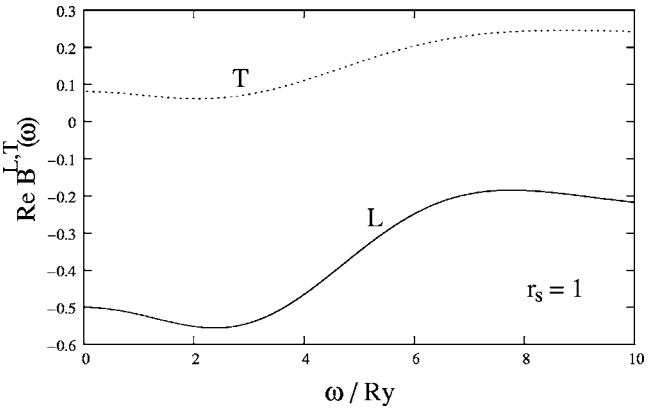

FIG. 6. Real part of $B^L(\omega)$ and $B^T(\omega)$ at $r_s=1$. Notations and units are as in Fig. 5.

$$\chi_s^{L,T}(q,\omega)=\frac{\chi_0^{L,T}(q,\omega)}{1-f_{xc,-}^{L,T}(q,\omega)\chi_0^{L,T}(q,\omega)q^2/\omega^2}, \tag{39}$$

which implies

$$\chi_0^{L,T}(q,\omega)\xrightarrow{q\to 0}\frac{n}{m}\left(1+\gamma^{L,T}\frac{E_F q^2}{m\omega^2}\right), \tag{40}$$

where $\gamma_L=3/2$ and $\gamma_T=1/2$. Comparing the $O(q^0)$ term of $\chi_s^{L,T}(q,\omega)$ in Eqs. (36) and (37) with the corresponding term in Eq. (40), we find

$$\frac{m_s}{m}=1-\lim_{\omega\to 0}\frac{n\,\mathrm{Re}\,A(\omega)}{m\omega^2}, \tag{41}$$

a result established in Ref. 30. Substituting Eq. (41) back into Eq. (39) yields

$$\chi_s^{L,T}(q,\omega)\xrightarrow{q\to 0}\frac{n}{m_s}\left[1+\gamma_{L,T}\frac{\epsilon_F q^2}{m_s\omega^2}+\frac{nq^2}{m_s\omega^2}B^{L,T}(\omega)\right]. \tag{42}$$

Comparison of Eq. (42) with Eqs. (36) and (37), respectively, leads to Eqs. (11) and (12), and to the further relation

$$B^L(0)-B^T(0)=\left.\frac{1}{n}\frac{\partial^2}{\partial\zeta^2}\epsilon_{xc}(\zeta)\right|_{\zeta=0}, \tag{43}$$

where $\epsilon_{xc}(\zeta)$ is the xc energy per particle at spin polarization ζ, and

$$\left.\frac{\partial^2}{\partial\zeta^2}\epsilon_{xc}(\zeta)\right|_{\zeta=0}=E_F\frac{F_0^a-F_1^s/2}{1+F_1^s/2}. \tag{44}$$

Equation (43) combined with the following relation for the charge-density channel:

$$\lim_{\omega\to 0}\frac{f_{xc}^L(\omega)-f_{xc}^T(\omega)-\partial^2(n\epsilon_{xc})/\partial n^2}{\omega}=0, \tag{45}$$

yields

$$\lim_{\omega\to 0}\frac{f_{\sigma\sigma'}^L(\omega)-f_{\sigma\sigma'}^T(\omega)-\partial^2(n\epsilon_{xc})/\partial n_\sigma\partial n_{\sigma'}}{\omega}=0. \tag{46}$$

Equation (45) is a 2D analog of Eq. (94) in Ref. 18, and obtained following an argument similar to that in Ref. 32.

IV. INTERPOLATION FORMULAS

Based on all the exact results listed in Sec. II, we give first an interpolation formula for $\mathrm{Im}\,A(\omega)$. We are somehow limited by the fact of the divergence of $\mathrm{Re}\,A(\omega)$ at limiting large frequency. In effect, Eq. (5) can be derived from Eq. (4), and thus it is not an independent result. In view of this limitation, we try the following simple formula:

$$\mathrm{Im}\,A(\omega)=\bar{\omega}^3\frac{a\ln|\bar{\omega}|-|\bar{\omega}|}{1+b\bar{\omega}^4}(2E_F), \tag{47}$$

where $\bar{\omega}=\omega/2E_F$. Equation (47) has the right low- and high-frequency behaviors of Eqs. (4) and (8) if one chooses the parameters to be

$$a=\frac{1}{3}\left(\frac{r_s}{r_s+\sqrt{2}}\right)^2, \tag{48}$$

and

$$b=\left(\frac{2}{\pi r_s}\right)^2. \tag{49}$$

Plots of $\mathrm{Im}\,A(\omega)$ and $\mathrm{Re}\,A(\omega)$ based on Eq. (47) are presented in Figs. 1–4.

Next, we present our interpolation formula for $\mathrm{Im}\,B^{L,T}(\omega)$,

TABLE I. ω_m in units of $2E_F$.

r_s	1	2	3	4	5
ω_m	1.208	1.728	2.040	2.276	2.519

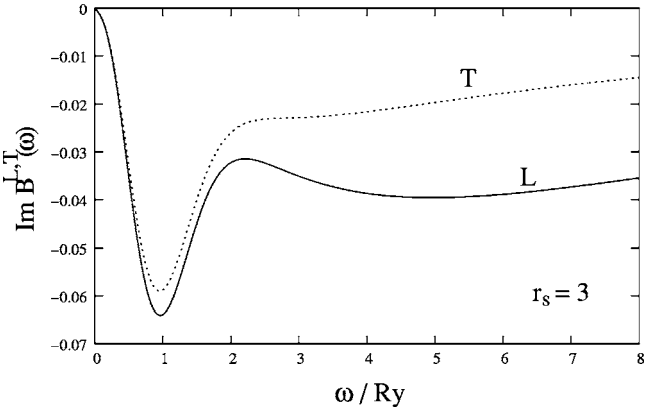

FIG. 7. Imaginary part of $B^L(\omega)$ and $B^T(\omega)$ at $r_s=3$. Notations and units are as in Fig. 5.

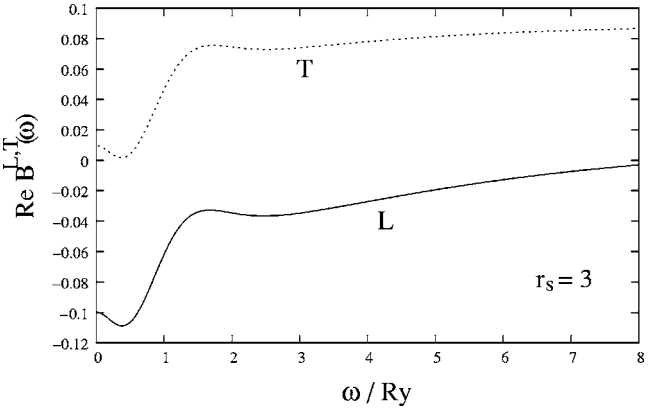

FIG. 8. Real part of $B^L(\omega)$ and $B^T(\omega)$ at $r_s=3$. Notations and units are as in Fig. 5.

$$\mathrm{Im}\, B^{L,T}(\omega) = -\frac{Ry}{n}\tilde{\omega}\left(\frac{a^{L,T}}{1+b^{L,T}\tilde{\omega}^2} + \tilde{\omega}^2 e^{-(|\tilde{\omega}|-\Omega^{L,T})^2/\Gamma^{L,T}}\right), \tag{50}$$

where $\tilde{\omega}=\omega/\omega_m$, with ω_m the position of the "collective peak."[18] The peak position of the contribution of plasmon excitations to $\mathrm{Im}\, B^{L,T}(\omega)$ can be roughly estimated in the same manner as in 3D. However, the estimation is not fully the same, due to the fact that the dispersion of the plasmon $\Omega_{pl}(k)$ starts with $\sim k^{1/2}$ at long wavelength in 2D rather than a constant. The contribution from the plasmons now starts from $\omega=0$ instead of $\omega=\omega_{pl}$, but it ends at $\Omega_{pl}(k)+[(k_F k+k^2)/2]/m$, as in the 3D case.[18] Therefore the up cutoff for the plasmon contribution is $2\Omega_{pl}(k_c)$, where k_c is the wave vector at which the plasmon enters the electron-hole continuum. The collective-mode contribution is therefore significant in the range $0\leqslant\omega<2\Omega_{pl}(k_c)$, and its maximum can be expected to occur roughly at about midrange $\omega_m=\Omega_{pl}(k_c)$. ω_m is given in Table I at several typical densities for the convenience of future applications.

The parameters appearing in Eq. (50) are determined as follows. Requiring that Eq. (50) has a peak at ω_m yields the relation

$$\Omega^{L,T} = 1 - \frac{3\Gamma^{L,T}}{2}. \tag{51}$$

The low-frequency limit of Eq. (13) fixes $a^{L,T}$ as

$$a^{L,T} = \frac{2\omega_m}{\pi E_F} S^{L,T}. \tag{52}$$

The high-frequency limit of Eq. (9) fixes $b^{L,T}$ as

$$b^{L,T} = \left(\frac{\omega_m}{\pi E_F}\right)^2 \frac{S^{L,T}}{c^{L,T}}. \tag{53}$$

Finally, from the Kramers-Krönig relation, we have

$$-\left(\frac{a^{L,T}}{\sqrt{b^{L,T}}} + \frac{1}{2\pi}\left\{2\Omega^{L,T}\Gamma^{L,T}e^{-(\Omega^{L,T})^2/\Gamma^{L,T}} + (\pi\Gamma^{L,T})^{1/2}[\Gamma^{L,T} + 2(\Omega^{L,T})^2]\left[1+\mathrm{erf}\left(\frac{\Omega^{L,T}}{\sqrt{\Gamma^{L,T}}}\right)\right]\right\}\right)\frac{Ry}{n} = \mathrm{Re}\, B^{L,T}(0) - \mathrm{Re}\, B^{L,T}(\infty), \tag{54}$$

where

$$\mathrm{erf}(x) = \frac{2}{\sqrt{\pi}}\int_0^x e^{-y^2} dy. \tag{55}$$

$\Gamma^{L,T}$ and $\Omega^{L,T}$ are further determined from Eqs. (51) and (54).

We now present numerical results for $\mathrm{Im}\, B^{L,T}(\omega)$ and $\mathrm{Re}\, B^{L,T}(\omega)$ at several typical densities. We use the Landau parameters based on a Monte Carlo calculation by Kwon, Ceperley, and Martin[33] to determine $B^{L,T}(0)$ via Eqs. (11) and (12). On the other hand, $B^{L,T}(\infty)$ is calculated from Eq. (10). We make use of the approximate correlation energy density ϵ_c proposed by Attaccalite *et al.*[34] to calculate t_c via the relation

TABLE II. Parameters for $\mathrm{Im}\, B^L(\omega)$ [Eq. (50)].

r_s	$10^2 a^L$	b^L	Γ^L	Ω^L
1	4.035	0.05517	0.5940	0.1090
2	2.272	0.04444	1.082	−0.6230
3	1.446	0.03339	1.334	−1.001
5	0.7692	0.02193	2.727	−3.091

TABLE III. Parameters for $\mathrm{Im}\, B^T(\omega)$ [Eq. (50)].

r_s	$10^2 a^T$	b^T	Γ^T	Ω^T
1	4.035	0.1655	0.9710	−0.4565
2	2.272	0.1333	1.177	−0.7655
3	1.446	0.1002	1.373	−1.060
5	0.7692	0.06579	1.698	−1.546

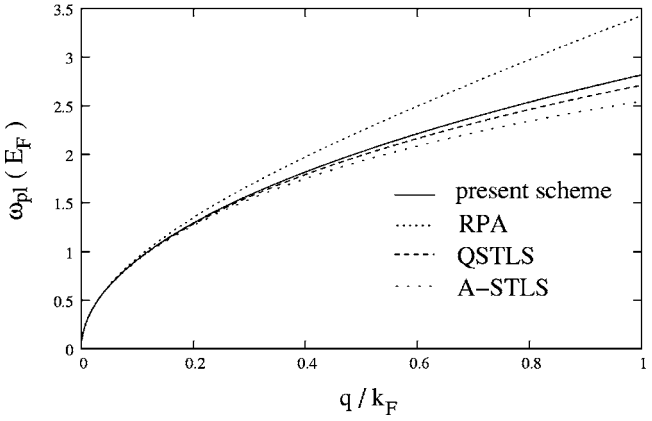

FIG. 9. The plasmon dispersion at $r_s=3$.

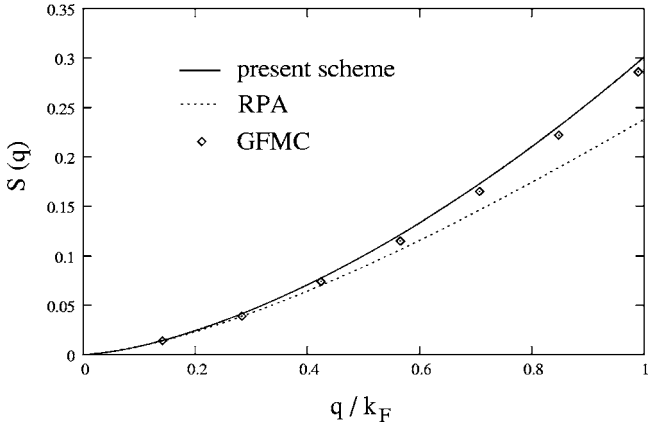

FIG. 10. The static structure factor at $r_s=5$.

$$t_c = -\epsilon_c - r_s \frac{d\epsilon_c}{dr_s}, \tag{56}$$

where ϵ_c is the correlation energy per particle. For the spin-resolved pair-correlation function $g_{\sigma\sigma'}(r)$, we use the values obtained by quantum Monte Carlo simulations by Gori-Giorgi, Moroni, and Bachelet in Table VIII of Ref. 35.

The values of the parameters in Eq. (50) are presented for four values of the Wigner-Seitz radius, $r_s=1$, 2, 3, and 5 in Tables II and III. It is necessary to mention here that the results for $B^{L,T}(\omega)$ based on the present interpolations also depend on the inputs, like the Landau parameters and the pair-correlation function, whose accuracy might not be always ensured at low density.

Plots of $\mathrm{Im}\, B^{L,T}(\omega)$ and $\mathrm{Re}\, B^{L,T}(\omega)$ for $r_s=1,3$ are presented in Figs. 5–8.

V. SUMMARY

The long-wavelength behavior of the dynamical spin-resolved exchange-correlation kernel in the two-dimensional electron liquid is studied. Several analytical results at limiting high and low frequency for its singular $A(\omega)$ and regular $B^{L,T}(\omega)$ components, in the long-wavelength expansion of Eq. (2), are obtained. These results are summarized, with those obtained previously in the literature, in Sec. II of this paper.

Based on these results, we have proposed interpolation formulas for $\mathrm{Im}\, A(\omega)$ and $\mathrm{Im}\, B^{L,T}(\omega)$ for all frequencies, from which we have also calculated $\mathrm{Re}\, A(\omega)$ and $\mathrm{Re}\, B^{L,T}(\omega)$ via the Kramers-Krönig relation. These formulas could be useful in the applications of time-dependent spin-density functional theory to the two-dimensional electron systems.

ACKNOWLEDGMENTS

The author thanks Dr. G. Vignale and Dr. S. M. Badalyan for discussions.

APPENDIX: PLASMON DISPERSION, STATIC STRUCTURE FACTOR, AND STATIC LOCAL-FIELD FACTOR

In this appendix, we employ the present scheme for the xc kernel (for the charge channel, we refer to Ref. 29) to calculate the plasmon dispersion, the static structure factor (SSF), and the static local-field factor (SLFF) of the electron liquid, properties that can be directly measured experimentally and/or have been extensively investigated theoretically.[4,5,36] Here, we compare such calculations with those previous results which are commonly believed to be quite accurate or relatively more reliable than random-phase approximation (RPA). Such a comparison can be carried out only in the small momentum regime, since our interpolations are only valid in this region. In fact, the comparison indicates that the present scheme is rather accurate, at least in this region.

First, we calculate the plasmon dispersion, which is determined by the following relation:

$$1 - [v(q) + \mathrm{Re}\, f_{xc}^{L}(q,\omega_{pl})]\mathrm{Re}\, \chi_0(q,\omega_{pl}) = 0. \tag{A1}$$

For small q, the plasmon frequency ω_{pl} in the preceding equation can be shown to be

$$\omega_{pl}^2 = \alpha q + \left[\beta + \frac{1}{\pi}\mathrm{Re}\, f_{xc}^{L}(0)E_F\right]q^2, \tag{A2}$$

where $\alpha=2E_Fe^2$, $\beta=3E_F/2m$, and $f_{xc}^{L}(0) = \lim_{\omega\to 0}\lim_{q\to 0} f_{xc}^{L}(q,\omega)$. It is understandable that only the charge channel of the xc kernel has effects on the plasmon dispersion, while the spin channel does not.

A comparison with analytical STLS (A-STLS) [Eq. (48) in Ref. 37]—which is basically equivalent to the self-consistent approach for SSF proposed by Singwi, Tosi, Land, and Sjölander (STLS)[24] but reformulates the latter in an analytical manner—at $r_s=3$ is shown in Fig. 9. Both the present scheme and the STLS give a big reduction to the well-known overestimated RPA result, which is also shown in Fig. 9 for a comparison. It is well recognized that the STLS is more accurate than the RPA. For example, it extends the r_s value for the non-negativity of the on-top pair-correlation density $g(0)$ to a much larger region than the RPA. Nevertheless, the classical type of framework and the use of the static local-field factor in the STLS might introduce drawbacks in its implementations, such as the violation of the compressibility sum rule. An issue relevant to the present subject is that the overestimation of the plasmon dispersion in the RPA result is believed to be over-reduced in the STLS. To obtain a better

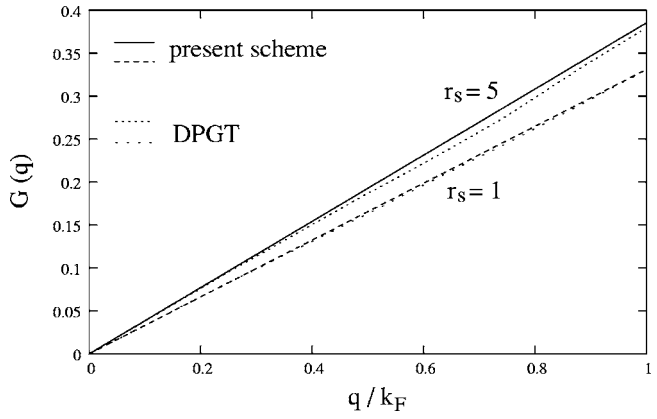

FIG. 11. The local field factor $G(q)$ for $r_s=1$ and $r_s=5$.

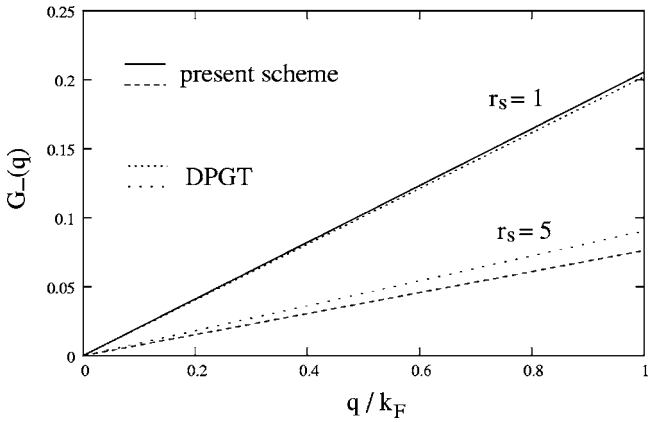

FIG. 12. The local field factor $G_-(q)$ for $r_s=1$ and $r_s=5$.

test of the accuracy of the present scheme, we further calculate the plasmon dispersion based on the quantum mechanical version of the STLS (QSTLS),[38,39] in which, for small q,

$$\omega_{pl}^2 = \alpha q + \left(\beta - \frac{e^2 k_F \gamma}{m}\right) q^2. \tag{A3}$$

Here

$$\gamma = -\frac{1}{2k_F}\int_0^\infty dq\big[S(q)-1\big], \tag{A4}$$

and values for it at several typical r_s are given in Ref. 39. The QSTLS is aimed at overcoming the shortcomings of the STLS, and a dynamic local-field factor is employed in it. We hence also show in Fig. 9 the plasmon dispersion calculated from Eq. (A3). It turns out that the results based on the present scheme and the QSTLS agree very well.

Next we calculate the SSF $S(q)$. It is well known that the plasmons in the electron liquid exhaust the contributions to the long-wavelength structure of $S(q)$,

$$S(q) = \frac{q^2}{2m\omega_{pl}}. \tag{A5}$$

Since $\omega_{pl}^2 \to \alpha q$, one has $S(q)=q^{3/2}/(2m\sqrt{\alpha})$ as $q\to 0$. In fact, it was shown that the single-pair and multipair electron-hole excitations make contributions to the order of $O(q^3)$ and $O(q^4)$, respectively.[40] The plasmon contributions fully determine the SSF to the order of $O(q^{5/2})$. From the the dissipation-fluctuation relation (Ref. 41),

$$S(q) = -\frac{1}{\pi n}\int_0^\infty d\omega\, \mathrm{Im}\,\chi(q,\omega), \tag{A6}$$

where $\chi(q,\omega)$ is the response function, one obtains

$$S(q) = \frac{q^2}{2m\omega_{p0}}\left[1 - \frac{3}{4}\frac{E_F q^2}{m\omega_{p0}^2} - \frac{1}{2}v(q)^{-1}\,\mathrm{Re}\,f_{xc}(\omega_{p0})\right], \tag{A7}$$

where $\omega_{p0}=\sqrt{\alpha q}$. We emphasize that the preceding result is accurate to $O(q^{5/2})$. We compare $S(q)$ with the result obtained by Green's-function Monte Carlo (GFMC) calculation[42] at $r_s=5$ in Fig. 10. Our result in Eq. (A7) agrees very well with the GFMC calculation. The RPA result, corresponding to putting $f_{xc}^L(\omega_{p0})=0$ in Eq. (A7), is also shown in Fig. 10 for comparison.

Finally, we calculate the SLFF, which is defined as

$$G(q) = -\frac{1}{v(q)}\lim_{q\to 0}\lim_{\omega\to 0} f_{xc}^L(q,\omega). \tag{A8}$$

To this end, it might be necessary to emphasize the fact that (Refs. 12, 32, and 43)

$$\lim_{\omega\to 0}\lim_{q\to 0} f_{xc}^{L,T}(q,\omega) \neq \lim_{q\to 0}\lim_{\omega\to 0} f_{xc}^{L,T}(q,\omega). \tag{A9}$$

In fact,

$$\lim_{q\to 0} G(q) = -\frac{1}{v(q)}[f_{xc}^L(\omega=0) - f_{xc}^T(\omega=0)], \tag{A10}$$

where $f_{xc}^{L,T}(\omega=0)=\lim_{\omega\to 0}\lim_{q\to 0} f_{xc}^{L,T}(q,\omega)$. Similarly, for the spin channel, one has

$$\lim_{q\to 0} G_-(q) = -\frac{1}{v(q)}[B^L(0) - B^T(0)]. \tag{A11}$$

We calculate, for small momentum q, $G(q)$ and $G_-(q)$ and compare them with the results of Davoudi *et al.* (DPGT),[44] which reproduce the diffusion Monte Carlo (DMC)[45] data. We plot $G(q)$ at $r_s=1$ and $r_s=5$ in Fig. 11. The agreement between the results based on our scheme and those based on the DPGT scheme is excellent. This is understandable because in both schemes, the Monte Carlo data of Ref. 46 for ϵ_{xc} is employed.

In Fig. 12, we show $G_-(q)$ at $r_s=1$ and $r_s=5$ and compare it with that of DPGT.[44] They turn out to be rather close. The difference arises from the fact that we have made use of the Monte Carlo data in Ref. 33 for the Landau parameters to calculate the quantity $(\partial^2/\partial\zeta^2)\epsilon_{xc}(\zeta)|_{\zeta=0}$ via Eq. (44), while DPGT calculated it by extrapolating the DMC data[45] for $G_-(q)$ to $q=0$.

[1] T. Ando, A. B. Fowler, and F. Stern, Rev. Mod. Phys. **54**, 437 (1982).
[2] For example, A. V. Chaplik, Zh. Eksp. Teor. Fiz. **60**, 1845 (1971) [Sov. Phys. JETP **33**, 997 (1971)]; A. K. Rajagopal and J. C. Kimball, Phys. Rev. B **15**, 2819 (1977); F. Stern, Phys. Rev. Lett. **18**, 546 (1967).
[3] J. Hubbard, Proc. R. Soc. London **243**, 336 (1957).
[4] K. S. Singwi, and M. P. Tosi, in *Solid State Physics*, edited by H. Ehrenreich, F. Seitz, and D. Turnbull (Academic, New York, 1981), Vol. 36, p. 177.
[5] S. Ichimaru, Rev. Mod. Phys. **54**, 1017 (1982).
[6] P. Hohenberg and W. Kohn, Phys. Rev. **136**, B864 (1964).
[7] W. Kohn and L. J. Sham, Phys. Rev. **140**, A1133 (1965).
[8] E. Runge and E. K. U. Gross, Phys. Rev. Lett. **52**, 997 (1984).
[9] E. K. U. Gross, J. F. Dobson, and M. Petersilka, in *Topics in Current Chemistry*, edited by R. F. Nalewajski (Springer, Berlin, 1996).
[10] G. Vignale and W. Kohn, Phys. Rev. Lett. **77**, 2037 (1996).
[11] G. Vignale and W. Kohn, in *Electronic Density Functional Theory*, edited by J. Dobson, M. P. Das and G. Vignale (Plenum Press, New York, 1996).
[12] G. Vignale, C. A. Ullrich, and S. Conti, Phys. Rev. Lett. **79**, 4878 (1997).
[13] Z. Qian, A. Constantinescu, and G. Vignale, Phys. Rev. Lett. **90**, 066402 (2003).
[14] P. L. de Boeij, F. Kootstra, J. A. Berger, R. van Leeuwen, and J. G. Snijders, J. Chem. Phys. **115**, 1995 (2001).
[15] M. van Faassen, P. L. de Boeij, R. van Leeuwen, J. A. Berger, and J. G. Snijders, Phys. Rev. Lett. **88**, 186401 (2002).
[16] M. van Faassen, P. L. de Boeij, J. Chem. Phys. **120**, 8353 (2004).
[17] M. van Faassen, P. L. de Boeij, J. Chem. Phys. **121**, 10707 (2004).
[18] Z. Qian and G. Vignale, Phys. Rev. B **68**, 195113 (2003).
[19] Z. Qian, Phys. Rev. B **70**, 235118 (2004).
[20] G. S. Atwal, I. G. Khalil, and N. W. Ashcroft, Phys. Rev. B **67**, 115107 (2003).
[21] G. S. Atwal and N. W. Ashcroft, Phys. Rev. B **67**, 233104 (2003).
[22] R. Nifosì, S. Conti, and M. P. Tosi, Phys. Rev. B **58**, 12758 (1998); S. Conti, R. Nifosì, and M. P. Tosi, J. Phys.: Condens. Matter **9**, L475 (1997).
[23] C. F. Richardson and N. W. Ashcroft, Phys. Rev. B **50**, 8170 (1994).
[24] For example, K. S. Singwi, M. P. Tosi, R. H. Land, and A. Sjölander, Phys. Rev. **176**, 589 (1968).
[25] Y. Takada, Phys. Rev. Lett. **87**, 226402 (2001).
[26] B. Dabrowski, Phys. Rev. B **34**, 4989 (1986).
[27] E. K. U. Gross and W. Kohn, Phys. Rev. Lett. **55**, 2850 (1985); **57**, 923 (1986).
[28] N. Iwamoto and E. K. U. Gross, Phys. Rev. B **35**, 3003 (1987).
[29] Z. Qian and G. Vignale, Phys. Rev. B **65**, 235121 (2002).
[30] Z. Qian, G. Vignale, and D. C. Marinescu, Phys. Rev. Lett. **93**, 106601 (2004).
[31] M. Hasegawa and W. Watabe, J. Phys. Soc. Jpn. **27**, 1393 (1969).
[32] C. A. Ullrich and G. Vignale, Phys. Rev. B **65**, 245102 (2002).
[33] Y. Kwon, D. M. Ceperley, and R. M. Martin, Phys. Rev. B **50**, 1684 (1994).
[34] C. Attaccalite, S. Moroni, P. Gori-Giorgi, and G. B. Bachelet, Phys. Rev. Lett. **88**, 256601 (2002); **91**, 109902(E) (2003).
[35] P. Gori-Giorgi, S. Moroni, and G. B. Bachelet, Phys. Rev. B **70**, 115102 (2004).
[36] For example, D. Pines, and D. Bohm, Phys. Rev. **92**, 609 (1953); W. Schülke, J. R. Schmitz, H. Schulte-Schrepping, and A. Kaprolat, Phys. Rev. B **52**, 11721 (1995); C. F. Hirjibehedin, A. Pinczuk, B. S. Dennis, L. N. Pfeiffer, and K. W. West, Phys. Rev. B **65**, 161309(R) (2002); Y. Takada and H. Yasuhara, Phys. Rev. Lett. **89**, 216402 (2002).
[37] A. Gold and L. Calmels, Phys. Rev. B **48**, 11622 (1993).
[38] A. Holas and S. Rahman, Phys. Rev. B **35**, 2720 (1987).
[39] R. K. Moudgil, P. K. Ahluwalia, and K. N. Pathak, Phys. Rev. B **52**, 11945 (1995).
[40] N. Iwamoto, Phys. Rev. A **30**, 3289 (1984).
[41] D. Pines and P. Nozières, *The Theory of Quantum Liquids* (Addison-Wesley, Reading, MA, 1989), Vol. 1.
[42] B. Tanatar and D. M. Ceperley, Phys. Rev. B **39**, 5005 (1989).
[43] S. Conti and G. Vignale, Phys. Rev. B **60**, 7966 (1999).
[44] B. Davoudi, M. Polini, G. F. Giuliani, and M. P. Tosi, Phys. Rev. B **64**, 153101 (2001); B. Davoudi, M. Polini, G. F. Giuliani, and M. P. Tosi, Phys. Rev. B **64**, 233110 (2001).
[45] S. Moroni, D. M. Ceperley, and G. Senatore, Phys. Rev. Lett. **69**, 1837 (1992); G. Senatore, S. Moroni, and D. Varsano, Solid State Commun. **119**, 333 (2001).
[46] F. Rapisarda and G. Senatore, Aust. J. Phys. **49**, 151 (1996).